

Generative Photography: Scene-Consistent Camera Control for Realistic Text-to-Image Synthesis

Yu Yuan¹, Xijun Wang¹, Yichen Sheng², Prateek Chennuri¹, Xingguang Zhang¹, Stanley Chan¹
¹School of ECE, Purdue University ²NVIDIA Research



Figure 1. This paper introduces generative photography, a new paradigm for text-to-image generation that maintains a consistent base scene while modifying only the camera settings to achieve varied photographic effects. Current state-of-the-art text-to-image generation models like Stable Diffusion 3 (SD3) [4] and FLUX [3] face two major limitations: the inability to accurately interpret camera-specific settings and the challenge of maintaining consistency in the base scene. This paper introduces a novel approach that addresses these issues, enabling precise camera setting control and consistent scenes in generative models.

Abstract

Image generation today can produce somewhat realistic images from text prompts. However, if one asks the generator to synthesize a particular camera setting such as creating different fields of view using a 24mm lens versus a 70mm lens, the generator will not be able to interpret and generate scene-consistent images. This limitation not only hinders the adoption of generative tools in photography applications but also exemplifies a broader issue of bridging the gap between the data-driven models and the physical world. In this paper, we introduce the concept of **Generative Photography**, a framework designed to control camera intrinsic settings during content generation. The core innovation of this work are the concepts of Dimensionality Lifting and Contrastive Camera Learning, which achieve continuous and consistent transitions for different camera settings. Experimental results show that our method produces significantly more scene-consistent photorealistic images than state-of-the-art models such as Stable Diffusion 3 and FLUX.

Generative Photography, a framework designed to control camera intrinsic settings during content generation. The core innovation of this work are the concepts of Dimensionality Lifting and Contrastive Camera Learning, which achieve continuous and consistent transitions for different camera settings. Experimental results show that our method produces significantly more scene-consistent photorealistic images than state-of-the-art models such as Stable Diffusion 3 and FLUX.

1. Introduction

Since the breakthrough of probabilistic diffusion models in the early 2020’s [15, 23, 51, 59], foundational vision models have created unprecedented opportunities for artificially generated content [3–5, 7, 17, 20, 33, 43, 49, 51–53, 72, 73].

[†]This work is supported, in part, by the National Science Foundation under grants 2133032, 2134209, 2030570, and 2431505.

[‡]Project page: <https://generative-photography.github.io/project/>.

Content generation processes that would have taken days of human labor in the past are now possible by machines in just a few seconds. However, while today’s text-to-image engines can generate somewhat realistic images, professional photographers still have many reservations about these tools because even the most basic camera effects cannot be produced. For example, the prompt “quiet mountain trail, 24mm lens” and another prompt “quiet mountain trail, 70mm lens” will have no differences in the field of view (FoV) but different rocks and trees, as illustrated in Fig. 1 (b).

The inability of current diffusion models to effectively comprehend camera settings is not merely a matter of scaling laws [29], but rather a fundamental disconnect between data-driven models and the physical world. Recent research [28] demonstrates that increasing training data and model parameters are insufficient for generation models to capture essential physics principles. To bridge this gap, we need to “teach physics” to the models. However, teaching physics is not a trivial task because we lack both training data and suitable mathematical tools to disentangle camera physics from the scene content. The goal of this paper is to propose a new framework, driven by a co-design of data and network architecture, to enable generative photography, specifically focusing on achieving image generation with intrinsic camera setting awareness.

What is Generative Photography? Generative photography is a new paradigm in photography where content is generated instead of captured. Generative photography stresses *camera-awareness*. On top of an existing text-to-image generation process, we demand the model to comprehend the typical camera settings: adjusting the aperture, shutter speed, focal length, and color temperature. By adjusting these camera settings, we can create a variety of photorealistic effects such as different bokeh effects, exposure, color, and zoom. A successful generative photography method should satisfy three objectives: (1) the camera effects are realistically rendered; (2) by changing the camera settings, the content of the scene is not altered, e.g., the buildings remain the same buildings and persons remain the same persons; (3) adding camera awareness does not degrade the image quality when compared to the baseline models that do not possess this property.

Why do Existing Models Fail? There are two primary reasons why existing generative models fail.

1. The available training data is very limited. To train a generative photography model, we need sets of images captured under different camera settings, such as varying apertures or focal lengths. Apart from the fact that acquiring these paired images is tedious and time/manpower-consuming, there is also a lack of tex-

tual labels. Therefore, in the absence of sufficient training data, it is challenging to train or fine-tune existing visual models.

2. Even if we have the training data, it remains unclear how one can disentangle the information of scene embeddings from the camera embeddings. If we cannot disentangle these embeddings, then it will be impossible to keep the scene unchanged while altering the camera settings. This would lead to severe scene consistency problems as illustrated in Fig. 1.

In this paper, we emphasize the concept of scene consistency from one camera setting to another camera setting. For example, if we change from “24mm lens” to “70mm lens”, there is a smooth transition from one field of view (FoV) to another. Such a smooth change creates a camera dimension, similar to the concept of spatial dimension and temporal dimension that we used to see. Therefore, to process this camera dimension, we should leverage two approaches:

- **Dimensionality Lifting.** We should lift the space-only problem to a space-camera joint problem. The lifting and the joint optimization will enable new disentanglement capabilities and ensure consistency.
- **Contrastive Camera Learning.** We should design a contrastive camera learning strategy to facilitate the generative model’s understanding of camera physics. This strategy operates at both the data and network levels, jointly emphasizing the changes introduced by varying camera settings within the same scene.

In summary, the contribution of this paper is two-fold:

1. We introduce the concept of Generative Photography, a new paradigm focusing on enabling text-to-image diffusion models with precise and consistent controllability over camera intrinsic settings.
2. To support generative photography, we present two new techniques, dimensionality lifting and contrastive camera learning, to allow scene-consistent camera control for realistic text-to-image generation. This framework can be used on various camera effects, producing appealing camera control with consistent scenes.

2. Prior Work and Limitations

2.1. Text-to-image Generation

Diffusion models [15, 23, 51, 59] have emerged as a powerful framework in the field of generative AI, primarily due to their robustness and versatility in generating high-quality images from textual descriptions. Tutorials such

as [9, 32, 39] have provided comprehensive coverage of the foundations of these diffusion models.

Notable implementations of text-to-image generation utilizing diffusion models include DALL-E [49], Stable Diffusion [4], DreamBooth [52], IMAGEN [53], FLUX [3], and others [17, 43, 51]. DALL-E pioneered the generation of novel images by combining concepts, attributes, and styles derived from textual input, demonstrating an advanced capability for understanding and creatively interpreting descriptions. Stable Diffusion further enhances this by generating high-resolution images in a latent space, significantly improving both computational efficiency and output quality.

2.2. Camera-Awareness

When we think about camera-aware content generation, a fundamental question is how to control the diffusion model so that it respects the camera settings. The following three families of approaches are the most relevant ones to us:

- **Camera-Awareness Via Guidance.** In theory, camera awareness can be done by integrating the control signals into the generation process through guidance. Methods such as ControlNet [73], T2I-Adapter [42], and GLIGEN [35] belong to this category where they use depth maps, edge maps, semantic maps, and object-bounding boxes to guide the diffusion process. However, this guidance is mostly about the *scene*, not the *camera*. We are interested in the latter.
- **Camera External Parameters.** Existing work related to our work mostly focuses on controlling the camera external parameters such as its pose and trajectory [6, 11, 13, 22, 25, 27, 34, 41, 62, 68, 69]. Approaches like CameraCtrl [22] and CamCo [69] incorporate these external parameters into pre-trained generative models by leveraging an additional camera encoder network. However, these methods are limited to single-camera trajectories, leading to significant inconsistencies in content and dynamics when generating multiple videos. Collaborative video diffusion (CVD) [34] and Civia [68] improve consistency by aligning features across multi-view video generation branches.
- **Camera Intrinsic Settings.** When it comes to intrinsic camera settings, there is very limited work except for some basic zoom-in/out effects [2, 7, 20, 60]. One of the main challenges is that most datasets used for training vision models often lack comprehensive camera settings. Even when some camera metadata is included, there is typically an absence of multi-setting metadata for the same scene. This lack of parameter variation means that the available metadata cannot fully capture the true physical meaning of these settings. For instance, for a given scene, having only a

single 50mm f/8 setting makes it difficult to infer how the depth of field (DoF) and field of view (FoV) would change under a 16mm f/4 setting for the same scene.

2.3. Information Disentanglement

Beyond the previous related works, a major difficulty in camera-aware content generation is the user-computer interface. In today’s text-to-image generation, a user needs to modify the prompt to control the image attributes. However, once the camera prompt is modified, the overall image structure can be severely distorted due to the sensitivity of outputs to the prompt-seed combination [18, 31, 52, 66]. This happens because we are not able to *disentangle* the camera embeddings and scene embeddings.

- **GAN-based Disentanglement.** Information disentanglement can be done in many ways. In the pre-diffusion era, generative adversarial networks (GANs) [19] have shown potential for highly disentangled control in their latent spaces, enabling precise manipulation of facial attributes without affecting others [30, 54–56, 61]. For example, StyleGAN [30, 61] allows detailed control over image properties through linear editing of its latent space, isolating specific attributes while preserving others.
- **Diffusion-based Disentanglement.** There is increasing evidence that diffusion models can perform some degree of latent space information disentanglement. For example, Wu *et al.* [66] did a case study about Stable Diffusion [4] and consequently proposed to optimize the text embeddings during inference to maintain image coherence. There are new mechanisms to explicitly enforce information disentanglement, e.g., Wu *et al.* [65] used contrastive guidance by sending two prompts to disentangle the information, and Rohit *et al.* [18] minimized interference by identifying a low-rank direction. The general problem of these approaches is that they are mostly tailored to facial attributes. When applying them to generic image content, they struggle with shapes and colors. Additionally, they primarily focus on optimizing the text embeddings during inference without considering any joint strategies to decouple data and models.

In this paper, we introduce the task of generative photography. We propose a framework consisting of two concepts: dimensionality lifting and contrastive camera learning, which disentangle camera and scene embeddings. Our framework enables precise control over various camera settings, such as shutter speed, aperture, focal length, and color temperature, while maintaining scene consistency, allowing for exposure, bokeh rendering, zoom, and color control in generated images. These aspects will be detailed in the proposed methods section.

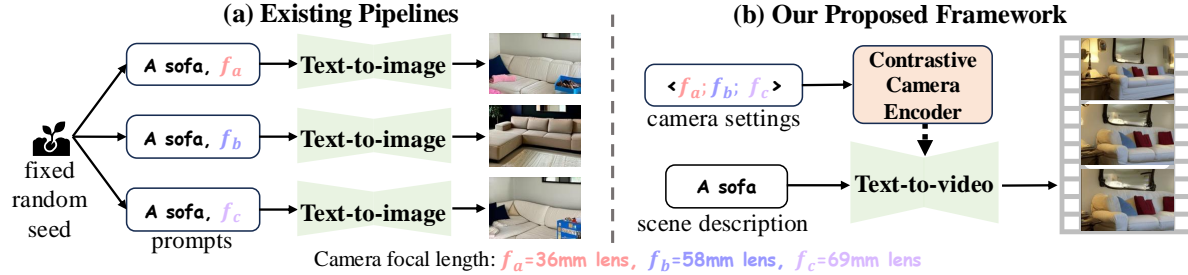


Figure 2. (a) Existing T2I models struggle to perceive physical camera settings and maintain consistency across multiple settings, even when the random seed is fixed. (b) We solve this problem by lifting camera-controlled text-to-image (T2I) generation into text-to-video (T2V) generation, thereby decoupling scene description from camera settings and achieving better scene consistency.

3. Proposed Methods

3.1. Dimensionality Lifting

A critical question in generative photography is how to disentangle the camera embedding from the scene embedding. Without this disentanglement, it becomes challenging to maintain consistency in the scene. In this paper, we first propose the idea of dimensionality lifting to achieve this. Figure 2 (a) illustrates the low consistency between generated images in existing text-to-image (T2I) generation processes, where only part of the prompt is modified (in this case, the camera focal length). This paper addresses this issue within a higher-dimensional text-to-video (T2V) paradigm. As shown in Fig. 2 (b), we lift multi-camera setting image generation with video generation. Within the T2V framework, we decouple the invariant scene description from camera settings: the scene description is used to establish a foundational scene, while the camera settings provide extra constraints for each corresponding frame.

There are several reasons why dimensionality lifting could solve our problem: (i) Variations in camera settings are important factors to consider; thus, we should elevate our base problem from a space-only problem to a space-camera joint problem. (ii) This approach allows for a modular separation between scene elements and camera settings, enabling more flexible and accurate manipulations of camera-related aspects without impacting the underlying scene structure. (iii) Video generation models, due to their spatiotemporal attention design, are inherently better at maintaining consistency across frames [7, 24, 58, 67]. (iv) We can leverage the powerful generative capabilities of pre-trained T2V models to ensure high-quality image generation.

3.2. Contrastive Camera Learning

Another challenge in generative photography is how to teach the model to understand the physical settings of a camera. To achieve this, we propose a contrastive camera learning approach, consisting of two primary components: contrastive data and contrastive camera encoder. On

the data side, we build a contrastive dataset that provides image-text pairs of a fixed scene under varying values of specific camera settings. At the network level, we inject the differences between adjacent camera settings to help the network further understand the impact of the variations.

3.2.1 Contrastive Data

The contrastive dataset provides data-driven support for camera settings understanding in generative tasks.

What is Contrastive Data and Why is it Useful? Contrastive data involves creating pairs or sets of images that highlight specific differences, such as varying camera settings, while keeping other elements constant. Contrastive data is advantageous as it enables models to focus on and learn from the differences between images, rather than being overwhelmed by the vast diversity of real-world data. Here is a simple example of contrastive data.

Example. If the images vary by color temperature, their corresponding textual labels might be:
 Invariant scene description: "A squirrel eating a leaf from a tree."
 Color temperature for each frame: $\langle 9933K; 3626K; 6302K; 4039K; 2400K \rangle$

How is the Contrastive Data Constructed? We propose to construct a contrastive dataset in three steps following the outline shown in Fig. 3.

(i). **Vision Language Model Captioning for Base Images:** To ensure that the data we generate can be used for training, we first need to collect base images and obtain their textual labels. The base images we select must be of high quality and meet specific requirements for camera generation tasks. For example, for shutter speed control, the base images should have a wide dynamic range and appropriate exposure; for color temperature control, all

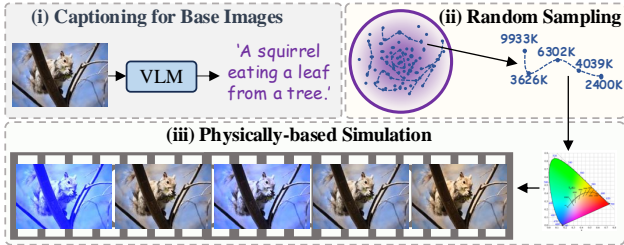


Figure 3. The pipeline of building contrastive data.

base images should lean towards a neutral color temperature; for bokeh rendering tasks, the base images should be all-in-focus images; and for focal length control, the base images need to have sufficiently high resolution. We employ a vision language model (VLM) LLaVA [37] to generate scene captions for a base image, which we use as the invariant scene descriptions for this contrastive set.

(ii). Random Sampling on Continuous Camera Space:

Camera settings are typically treated as continuous variables, such as focal length, shutter speed, and color temperature. We argue that each value on the camera setting scale is crucial, as it embodies a deeper physical understanding rather than merely representing a few discrete values. Continuous sampling supports continuous-scale training [8, 10, 64], which enhances the model’s ability to perform across any value on the scale. Therefore, when constructing contrastive data, we perform random sampling across the continuous camera setting scale to gather multiple values. Specifically, as shown in Fig. 3, we assume an *invariant scene description* on a continuous camera setting scale (here exemplified by color temperature, with the vertical axis representing color temperature). For each instance, we sample several (5 here) points along the horizontal axis and use this collection of points as a set to describe camera setting variations. We did not order the randomly collected data points in each set, ensuring that our network does not merely fit a specific directional pattern (such as simple zoom in/out for focal length) but instead learns the numerical values themselves. For the camera’s color temperature, we collect a range from 2,000 to 10,000 Kelvin. For shutter speed, we re-normalize it to a scale of 0.1 to 1.0 (where larger values correspond to brighter images). For focal length, we sample values between 24 mm and 70 mm. Regarding bokeh rendering, we sample blur parameter values from 1 to 30, with larger values corresponding to stronger blur effects.

(iii). Physically-based Simulation: In the context of physically-based simulation, after obtaining the randomly sampled camera settings, we render the corresponding frames based on physical simulation for the base image.

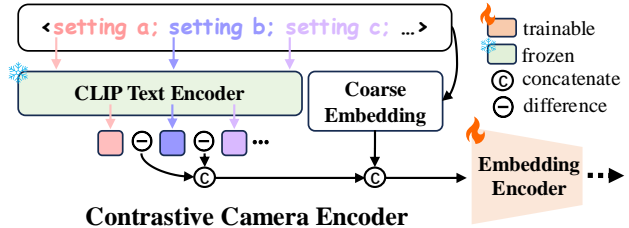


Figure 4. The overall architecture of contrastive camera encoder.

- Bokeh rendering [45, 46, 57]: We first extract the base image’s depth map using a depth estimation model Depth Anything [70, 71] and convert it to a disparity map, which, together with the base image and the sampled blur parameter, is input to the bokeh rendering module [45]. During this process, the refocused disparity remains fixed at the foreground depth, ensuring the foreground subject remains sharp while only adjusting the background blur.
- Focal length: We draw on Level-of-Detail methods [40, 63]; specifically, for a given high-resolution base image, we calculate the field of view (FoV) ratio [50] corresponding to the sampled focal length relative to the original focal length (thus the sampled focal length must exceed the base focal length). Based on this ratio, we center-crop the corresponding region from the base image and subsequently resize all images captured at different focal lengths to the same resolution.
- Shutter speed: We obtain images at different exposure levels by adjusting the captured image irradiance and converting it back to RGB images using a simulated image signal processor (ISP) [36].
- Color temperature: We adjust the RGB channel ratios according to the relationship between blackbody radiation and color temperature using empirical approximation [14] to fit various color temperatures.

Through the aforementioned steps, we obtain multiple frames corresponding to variations in camera settings, along with the associated invariant scene description and camera settings. For further details, please refer to the appendix.

3.2.2 Contrastive Camera Encoder

As shown in Fig 2 (b), after dimensionality lifting, we use the scene description as the primary input to the T2V model to represent the base scene, with the camera settings as additional conditions. These settings are fed into the Contrastive Camera Encoder, which injects them into the foundation models to control the camera effects for each frame. In the contrastive camera encoder, we enhance the network’s ability to understand and generate camera settings by embed-

ding camera settings and providing additional differential information.

As illustrated in Fig. 4, for each frame’s camera setting, we first create a coarse embedding, which incorporates a physical prior at the multi-channel pixel level (details in Appendix), similar to our physically-based simulation approach. Additionally, we capture inter-frame differences among camera settings as an auxiliary input to introduce finer-grained semantic difference information. Specifically, we utilize a frozen CLIP text encoder [48] to generate camera features for each frame and compute the feature differences between adjacent values of camera settings.

We then concatenate the coarse embedding with these differential features and feed them into an embedding encoder specifically designed for videos, similar to the T2I-Adaptor [42]. The embedding encoder and the T2V foundation encoder are structurally similar, which facilitates the integration of the multi-level features obtained from the embedding encoder into the foundation models. Following recommendations from CameraCtrl [22], we avoid using ControlNet [73] to mitigate information leakage issues.

We propose that the Contrastive Camera Encoder enhances the model’s ability to differentiate camera settings by focusing on comparative effects between them. This approach moves beyond a solely data-driven paradigm, significantly reducing the training data requirements and computational costs, while providing the network with more robust and precise control capabilities.

4. Experiments

In this section, we evaluate the application of our proposed framework in generative photography. Section 4.1 presents implementation details, Section 4.2 compares our framework with other potential methods, and Section 4.3 discusses the results of ablation studies.

4.1. Implementation Details

Datasets. As mentioned in Sub-section 3.2.1, we need high-quality base images with task-related features to simulate camera effects. For the exposure and white balance conditioning tasks, our base images are sourced from our own photography as well as public image datasets [44, 75]. For the bokeh rendering task, we collected all-in-focus base images from our own photography and [16, 21, 76], ensuring they contained a well-defined foreground subject with a distinguishable background. For the focal length task, our base images were sourced from our own photography and [16, 75], with all images captured using a full-frame camera equipped with a 24mm lens. The base images for focal task have a minimum resolution of 3,000 on the shorter side to ensure high quality and detailed high-frequency in-

formation, even after partial central cropping.

Each task includes 1,000 images with diverse scenes and varied shooting conditions. Note that these datasets are scalable, though we found 1,000 images sufficient to achieve the desired camera control effects.

Training and Inference. In this work, we select AnimateDiff [20] as our T2V base model, reducing the generated video frames to 5 to decrease computational costs for both training and inference. During training, most parameters of AnimateDiff are kept frozen, with only the motion LoRA [26] and our contrastive camera encoder being fine-tuned/trained. We use a learning rate of $1e-4$ with the Adam optimizer. The video resolution for training is set to 256×384 . For each task, we train with a batch size of 8 for 25,000 epochs, taking approximately 10 hours on an Nvidia A100 80GB GPU.

During inference, we input a prompt along with a set of camera settings to generate multiple frames. It’s worth noting that inference can also be conducted with a single camera setting by replicating this value across multiple frames, which results in a static output across frames. For bokeh rendering inference, no depth map is required.

Metrics. Our evaluation metrics primarily focus on accuracy to physical laws and scene consistency. The accuracy of generated images with respect to camera physical settings is evaluated using the Pearson correlation coefficient (CorrCoef) of trend changes between the generated images and the reference video. For scene consistency, we use frame-wise Learned Perceptual Image Patch Similarity (LPIPS) [74] to calculate the perceptual feature distance between frames generated with different camera settings. Additionally, to evaluate the impact of added camera controls on generation quality, we use CLIP [48] to compute the similarity score between generated images and the text prompt. For more details on the metrics, please refer to the supplementary material.

For each task, we chose 75 sets of camera settings for testing. These sets emphasize a wide range settings to enhance the robustness and persuasiveness of the evaluation.

4.2. Comparisons with Other Methods

To evaluate our method, we conduct comparisons against three categories of approaches: first, the state-of-the-art text-to-image generation models, Stable Diffusion 3 (SD3) [4] and FLUX [3]; second, the text-to-video generation model, AnimateDiff [20], fine-tuned on our contrastive dataset to assess the performance of a purely data-driven approach; and finally, CameraCtrl [22], where we adapt the model to control intrinsic camera settings instead of external ones, and train it on our dataset. Together, these baseline models form a comprehensive evaluation framework,

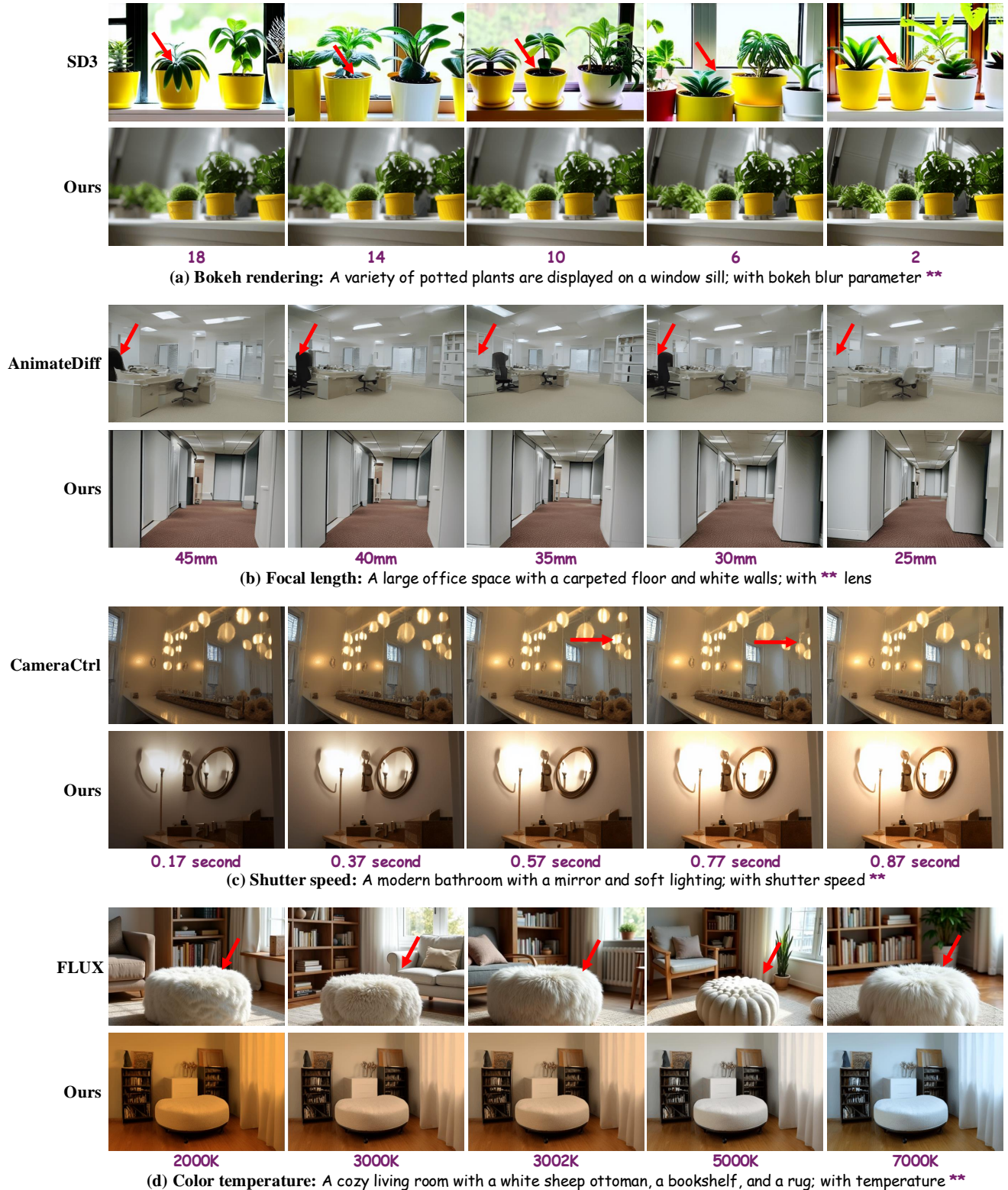


Figure 5. Visual comparisons between different generative methods. Our method is capable of generating realistic camera effects for any given camera setting scale, while maintaining high scene consistency across images corresponding to different scales. Both AnimateDiff [20] and CameraCtrl [22] have been fine-tuned on our data. We highlight the discontinuities in the scene with red arrows.

Methods	Bokeh Rendering			Focal Length			Shuttle Speed			Color Temperature		
	Accuracy CorrCoef ↑	Consistency LPIPS	Quality CLIP ↑	Accuracy CorrCoef ↑	Consistency LPIPS	Quality CLIP ↑	Accuracy CorrCoef ↑	Consistency LPIPS	Quality CLIP ↑	Accuracy CorrCoef ↑	Consistency LPIPS	Quality CLIP ↑
<i>Reference</i>	1.0000	0.0527	0.3974	1.0000	0.4709	0.3853	1.0000	0.0511	0.3783	1.0000	0.0398	0.4053
SD3 [4]	0.2492	0.7253	0.3278	0.2356	0.7108	0.3097	0.2731	0.6937	0.3169	0.2312	0.6891	0.3276
FLUX [3]	0.2006	0.6770	0.3257	0.2003	0.6461	0.3086	0.2398	0.6403	0.3192	0.2363	0.6155	0.3207
AnimateDiff [20] (w/o FT)	0.2960	0.1005	0.2753	0.2613	0.1208	0.2532	0.1843	0.1002	0.2631	0.1834	0.0805	0.2659
AnimateDiff [20] (w/ FT)	0.3714	0.0255	0.2984	0.2597	0.2288	0.2739	0.2198	0.0948	0.2936	0.2897	0.0205	0.2839
CameraCtrl [22] (w/o FT)	0.3303	0.1447	0.2804	0.2913	0.1144	0.2644	0.1896	0.0986	0.2912	0.1773	0.0935	0.2753
CameraCtrl [22] (w/ FT)	0.6025	0.1158	0.3017	0.8671	0.4606	0.2865	0.7526	0.0775	0.2981	0.5812	0.0651	0.2885
Ours	0.8626	0.0788	0.3007	0.9695	0.4647	0.2871	0.9264	0.0695	0.3015	0.8970	0.0499	0.2910

Table 1. Quantitative comparison with different generative methods. Accuracy is computed by comparing with reference videos; Consistency by frame-wise LPIPS; Quality by CLIP. *Reference* refers to the results obtained from physical simulations. *FT* denotes fine-tuning on our contrastive data. We highlight the **best** and **second-best** values for each metric

Methods	Bokeh Rendering			Focal Length			Shuttle Speed			Color Temperature		
	Accuracy CorrCoef ↑	Consistency LPIPS	Quality CLIP ↑	Accuracy CorrCoef ↑	Consistency LPIPS	Quality CLIP ↑	Accuracy CorrCoef ↑	Consistency LPIPS	Quality CLIP ↑	Accuracy CorrCoef ↑	Consistency LPIPS	Quality CLIP ↑
<i>Reference</i>	1.0000	0.0527	0.3974	1.0000	0.4709	0.3853	1.0000	0.0511	0.3783	1.0000	0.0398	0.4053
w/o contrastive	0.7631	0.1239	0.2964	0.8594	0.4943	0.2885	0.8864	0.0698	0.3007	0.8586	0.0699	0.2904
Discrete	0.6774	0.0854	0.2948	0.7254	0.4173	0.2833	0.8384	0.0584	0.2976	0.8140	0.0524	0.2946
Ours (3 frames)	0.8355	0.0814	0.2895	0.9273	0.3921	0.2857	0.9073	0.0685	0.2873	0.8848	0.0835	0.2955
Ours (5 frames)	0.8626	0.0788	0.3007	0.9695	0.4647	0.2871	0.9264	0.0695	0.3015	0.8970	0.0499	0.2980
Ours (7 frames)	0.8835	0.0747	0.2988	0.9783	0.4813	0.2909	0.9294	0.0535	0.3034	0.9095	0.0581	0.2985

Table 2. Quantitative results of ablation study.

encompassing image and video generation, external camera parameter control, and other related aspects.

In Fig. 5 demonstrates that our method generates images with excellent scene consistency, while realistically simulating camera effects based on any given setting value. Notably, in bokeh rendering, although no depth information was provided during inference, the rendered scenes appear to exhibit depth awareness, consistently keeping the foreground sharp while only the background varies according to the bokeh blur parameter. In color temperature control, our model also shows fine-grained control capabilities, producing images at 3,000K and 3,002K with only minimal differences in color temperature. From Table 1, although SD3 and FLUX demonstrate a clear advantage in generation quality, it exhibits lower consistency and accuracy between frames with different camera settings. After fine-tuning using our comparative dataset, both AnimateDiff and CameraCtrl showed obvious improvements in accuracy. Our method shows a significant advantage in both the accuracy and consistency of generated camera settings. It also performs well in generation quality, suggesting that our approach maintains the model’s overall generative capabilities without significant compromise. Here, a lower LPIPS score is not always better, as variations in color temperature, exposure, focal length, and bokeh can affect frame differences. The key metric is proximity to the reference videos.

4.3. Ablation study

Contrastive Camera Encoder. To assess the impact of contrastive network design, we removed inter-frame dif-

ferences in the contrastive camera encoder. Table 2 (w/o contrastive) suggests that incorporating different information enhances the model’s accuracy and consistency.

Data Sampling Strategy. To evaluate the impact of continuous data sampling in constructing the dataset, we compared it with the discrete (uniform) sampling method using 100 data points. Table 2 (Discrete) demonstrates that continuous sampling of data points better facilitates the network’s understanding of these physical values.

Number of Frames. Our model can perform training and inference across different frame counts. To assess the potential impact of varying training frames, we trained our model using 3, 5, and 7 frames. As shown in Table 2, increasing the frame number tends to improve the model’s accuracy and consistency. This also highlights a trade-off: while a higher number of camera settings offers users more options and improved performance, it also increases computational cost and processing time.

5. Conclusions

Generative photography opens the door to a new paradigm in photography where the generated contents are consistent with the intrinsic camera physics. Our solution is based on two concepts: dimensionality lifting and contrastive camera learning. It generates physically realistic camera effects while maintaining a high degree of scene consistency. Generative photography has the potential to reduce the post-processing burden in human-operated photography fundamentally. In addition, it offers a fresh perspective for generative models to understand the world better.

References

- [1] Brute-Force Matcher. https://docs.opencv.org/4.x/dc/dc3/tutorial_py_matcher.html. 14
- [2] Creating with camera control on gen-3 alpha turbo. <https://help.runwayml.com/hc/en-us/articles/34926468947347-creating-with-camera-control-on-gen-3-alpha-turbo>. 3
- [3] FLUX. <https://github.com/black-forest-labs/flux>. 1, 3, 6, 8
- [4] Stable Diffusion. <https://github.com/Stability-AI/StableDiffusion>. 1, 3, 6, 8
- [5] Video generation models as world simulators. <https://openai.com/index/video-generation-models-as-world-simulators/>. 1
- [6] Sherwin Bahmani, Ivan Skorokhodov, Aliaksandr Siarohin, Willi Menapace, Guocheng Qian, Michael Vasilkovsky, Hsin-Ying Lee, Chaoyang Wang, Jiayu Zou, Andrea Tagliasacchi, David B. Lindell, and Sergey Tulyakov. VD3D: Taming large video diffusion transformers for 3d camera control. *arXiv preprint arXiv:2407.12781*, 2024. 3
- [7] Andreas Blattmann, Tim Dockhorn, Sumith Kulal, Daniel Mendelevitch, Maciej Kilian, Dominik Lorenz, Yam Levi, Zion English, Vikram Voleti, Adam Letts, Varun Jampani, and Robin Rombach. Stable video diffusion: Scaling latent video diffusion models to large datasets. *arXiv preprint arXiv:2311.15127*, 2023. 1, 3, 4
- [8] Lucy Chai, Michael Gharbi, Eli Shechtman, Phillip Isola, and Richard Zhang. Any-resolution training for high-resolution image synthesis. In *European Conference on Computer Vision*, 2022. 5
- [9] Stanley H. Chan. Tutorial on diffusion models for imaging and vision. *arXiv preprint arXiv:2403.18103*, 2024. 3
- [10] Yinbo Chen, Oliver Wang, Richard Zhang, Eli Shechtman, Xiaolong Wang, and Michael Gharbi. Image neural field diffusion models. In *IEEE/CVF Conference on Computer Vision and Pattern Recognition*, pages 8007–8017, 2024. 5
- [11] Soon Yau Cheong, Duygu Ceylan, Armin Mustafa, Andrew Gilbert, and Chun-Hao Paul Huang. Boosting camera motion control for video diffusion transformers. *arXiv preprint arXiv:2410.10802*, 2024. 3
- [12] Yiheng Chi, Xingguang Zhang, and Stanley H. Chan. HDR imaging with spatially varying signal-to-noise ratios. In *IEEE/CVF Conference on Computer Vision and Pattern Recognition*, pages 5724–5734, 2023. 12
- [13] Robin Courant, Nicolas Dufour, Xi Wang, Marc Christie, and Vicky Kalogeiton. E.T. the exceptional trajectories: Text-to-camera-trajectory generation with character awareness. *arXiv preprint arXiv:2407.01516*, 2024. 3
- [14] Mark D. Fairchild. *Color Appearance Models*. 2013. 5, 13
- [15] Prafulla Dhariwal and Alexander Nichol. Diffusion models beat gans on image synthesis. In *Advances in Neural Information Processing Systems*, volume 34, 2021. 1, 2
- [16] Egor Ershov, Alexander Belokopytov, and Alex Savchik. Problems of dataset creation for light source estimation. *arXiv preprint arXiv:2006.02692*, 2020. 6
- [17] Rinon Gal, Yuval Alaluf, Yuval Atzmon, Or Patashnik, Amit H. Bermano, Gal Chechik, and Daniel Cohen-Or. An image is worth one word: Personalizing text-to-image generation using textual inversion, 2022. 1, 3
- [18] Rohit Gandikota, Joanna Materzyńska, Tingrui Zhou, Antonio Torralba, and David Bau. Concept Sliders: Lora adaptors for precise control in diffusion models. *arXiv preprint arXiv:2311.12092*, 2023. 3
- [19] Ian Goodfellow, Jean Pouget-Abadie, Mehdi Mirza, Bing Xu, David Warde-Farley, Sherjil Ozair, Aaron Courville, and Yoshua Bengio. Generative adversarial nets. In *Advances in Neural Information Processing Systems*, volume 27, 2014. 3
- [20] Yuwei Guo, Ceyuan Yang, Anyi Rao, Zhengyang Liang, Yaohui Wang, Yu Qiao, Maneesh Agrawala, Dahua Lin, and Bo Dai. AnimateDiff: Animate your personalized text-to-image diffusion models without specific tuning. *International Conference on Learning Representations*, 2024. 1, 3, 6, 7, 8, 16, 17, 18, 19
- [21] Samuel W. Hasinoff, Dillon Sharlet, Ryan Geiss, Andrew Adams, Jonathan T. Barron, Florian Kainz, Jiawen Chen, and Marc Levoy. Burst photography for high dynamic range and low-light imaging on mobile cameras. *ACM Transactions on Graphics*, 35(6), 2016. 6
- [22] Hao He, Yinghao Xu, Yuwei Guo, Gordon Wetzstein, Bo Dai, Hongsheng Li, and Ceyuan Yang. CameraCtrl: Enabling camera control for text-to-video generation. *arXiv preprint arXiv:2404.02101*, 2024. 3, 6, 7, 8, 16, 17, 18, 19
- [23] Jonathan Ho, Ajay Jain, and Pieter Abbeel. Denoising diffusion probabilistic models. In *Advances in Neural Information Processing Systems*, page 6840–6851, 2020. 1, 2
- [24] Jonathan Ho, Tim Salimans, Alexey Gritsenko, William Chan, Mohammad Norouzi, and David J Fleet. Video diffusion models. In *Advances in Neural Information Processing Systems*, volume 35, pages 8633–8646, 2022. 4
- [25] Chen Hou, Guoqiang Wei, Yan Zeng, and Zhibo Chen. Training-free camera control for video generation. *arXiv preprint arXiv:2406.10126*, 2024. 3
- [26] Edward J. Hu, Yelong Shen, Phillip Wallis, Zeyuan Allen-Zhu, Yuanzhi Li, Shean Wang, Lu Wang, and Weizhu Chen. LoRA: Low-rank adaptation of large language models. *arXiv preprint arXiv: 2106.09685*, 2021. 6
- [27] Hongda Jiang, Xi Wang, Marc Christie, Libin Liu, and Baoquan Chen. Cinematographic camera diffusion model. *Computer Graphics Forum*, 43(2), 2024. 3
- [28] Bingyi Kang, Yang Yue, Rui Lu, Zhijie Lin, Yang Zhao, Kaixin Wang, Gao Huang, and Jiashi Feng. How far is video generation from world model: A physical law perspective. *arXiv preprint arXiv: 2411.02385*, 2024. 2
- [29] Jared Kaplan, Sam McCandlish, Tom Henighan, Tom B. Brown, Benjamin Chess, Rewon Child, Scott Gray, Alec Radford, Jeffrey Wu, and Dario Amodei. Scaling laws for neural language models. *arXiv preprint arXiv: 2001.08361*, 2020. 2
- [30] Tero Karras, Samuli Laine, and Timo Aila. A style-based generator architecture for generative adversarial networks. In *IEEE/CVF Conference on Computer Vision and Pattern Recognition*, June 2019. 3

- [31] Bahjat Kawar, Shiran Zada, Oran Lang, Omer Tov, Huiwen Chang, Tali Dekel, Inbar Mosseri, and Michal Irani. Imagic: Text-based real image editing with diffusion models. In *IEEE/CVF Conference on Computer Vision and Pattern Recognition*, pages 6007–6017, 2023. 3
- [32] Diederik P. Kingma and Max Welling. An introduction to variational autoencoders. *arXiv preprint arXiv:1906.02691*, 2019. 3
- [33] Dan Kondratyuk, Lijun Yu, Xiuye Gu, José Lezama, Jonathan Huang, Grant Schindler, Rachel Hornung, Vignesh Birodkar, Jimmy Yan, Ming-Chang Chiu, Krishna Somandepalli, Hassan Akbari, Yair Alon, Yong Cheng, Josh Dillon, Agrim Gupta, Meera Hahn, Anja Hauth, David Hendon, Alonso Martinez, David Minnen, Mikhail Sirotenko, Kihyuk Sohn, Xuan Yang, Hartwig Adam, Ming-Hsuan Yang, Irfan Essa, Huisheng Wang, David A. Ross, Bryan Seybold, and Lu Jiang. VideoPoet: A large language model for zero-shot video generation. *arXiv preprint arXiv:2312.14125*, 2023. 1
- [34] Zhengfei Kuang, Shengqu Cai, Hao He, Yinghao Xu, Hongsheng Li, Leonidas Guibas, and Gordon. Wetzstein. Collaborative video diffusion: Consistent multi-video generation with camera control. In *arXiv preprint arXiv:2405.17414*, 2024. 3
- [35] Yuheng Li, Haotian Liu, Qingyang Wu, Fangzhou Mu, Jianwei Yang, Jianfeng Gao, Chunyuan Li, and Yong Jae Lee. GLIGEN: Open-set grounded text-to-image generation. *IEEE/CVF Conference on Computer Vision and Pattern Recognition*, 2023. 3
- [36] Zhihao Li, Ming Lu, Xu Zhang, Xin Feng, M. Salman Asif, and Zhan Ma. Efficient visual computing with camera raw snapshots. *IEEE Transactions on Pattern Analysis and Machine Intelligence*, 46(7):4684–4701, 2024. 5, 12
- [37] Haotian Liu, Chunyuan Li, Qingyang Wu, and Yong Jae Lee. Visual instruction tuning, 2023. 5
- [38] David G. Lowe. Distinctive image features from scale-invariant keypoints. *International Journal of Computer Vision*, 60(2):91–110, 2004. 14
- [39] Calvin Luo. Understanding diffusion models: A unified perspective. *arXiv preprint arXiv:2208.11970*, 2022. 3
- [40] S.G. Mallat. A theory for multiresolution signal decomposition: the wavelet representation. *IEEE Transactions on Pattern Analysis and Machine Intelligence*, 11(7):674–693, 1989. 5, 12
- [41] Andrew Marmon, Grant Schindler, José Lezama, Dan Kondratyuk, Bryan Seybold, and Irfan Essa. CamViG: Camera aware image-to-video generation with multimodal transformers. *arXiv preprint arXiv:2405.13195*, 2024. 3
- [42] Chong Mou, Xintao Wang, Liangbin Xie, Yanze Wu, Jian Zhang, Zhongang Qi, Ying Shan, and Xiaoou Qie. T2i-adapter: Learning adapters to dig out more controllable ability for text-to-image diffusion models. *arXiv preprint arXiv:2302.08453*, 2023. 3, 6, 14
- [43] Alexander Quinn Nichol, Prafulla Dhariwal, Aditya Ramesh, Pranav Shyam, Pamela Mishkin, Bob McGrew, Ilya Sutskever, and Mark Chen. GLIDE: Towards photorealistic image generation and editing with text-guided diffusion models. In *International Conference on Machine Learning*, pages 16784–16804, 2022. 1, 3
- [44] Hao Ouyang, Zifan Shi, Chenyang Lei, Ka Lung Law, and Qifeng Chen. Neural camera simulators. In *IEEE/CVF Conference on Computer Vision and Pattern Recognition*, 2021. 6
- [45] Juewen Peng, Zhiguo Cao, Xianrui Luo, Hao Lu, Ke Xian, and Jianming Zhang. BokehMe: When neural rendering meets classical rendering. In *IEEE/CVF International Conference on Computer Vision and Pattern Recognition*, 2022. 5, 12
- [46] Juewen Peng, Jianming Zhang, Xianrui Luo, Hao Lu, Ke Xian, and Zhiguo Cao. MPIB: An mpi-based bokeh rendering framework for realistic partial occlusion effects. In *European Conference on Computer Vision*, 2022. 5
- [47] Xiangyu Qu, Yiheng Chi, and Stanley H. Chan. Spatially varying exposure with 2-by-2 multiplexing: Optimality and universality. *IEEE Transactions on Computational Imaging*, 10:261–276, 2024. 12
- [48] Alec Radford, Jong Wook Kim, Chris Hallacy, Aditya Ramesh, Gabriel Goh, Sandhini Agarwal, Girish Sastry, Amanda Askell, Pamela Mishkin, Jack Clark, Gretchen Krueger, and Ilya Sutskever. Learning transferable visual models from natural language supervision. *CoRR*, abs/2103.00020, 2021. 6, 15
- [49] Aditya Ramesh, Mikhail Pavlov, Gabriel Goh, Scott Gray, Chelsea Voss, Alec Radford, Mark Chen, and Ilya Sutskever. Zero-shot text-to-image generation. In *International Conference on Machine Learning*, 2021. 1, 3
- [50] S.F. Ray. *Applied Photographic Optics: Lenses and Optical Systems for Photography, Film, Video, Electronic and Digital Imaging*. 2002. 5
- [51] Robin Rombach, Andreas Blattmann, Dominik Lorenz, Patrick Esser, and Björn Ommer. High-resolution image synthesis with latent diffusion models. In *IEEE/CVF Conference on Computer Vision and Pattern Recognition*, pages 10674–10685, 2022. 1, 2, 3
- [52] Nataniel Ruiz, Yuanzhen Li, Varun Jampani, Yael Pritch, Michael Rubinstein, and Kfir Aberman. DreamBooth: Fine tuning text-to-image diffusion models for subject-driven generation. In *IEEE/CVF Conference on Computer Vision and Pattern Recognition*, pages 22500–22510, 2023. 1, 3
- [53] Chitwan Saharia, William Chan, Saurabh Saxena, Lala Lit, Jay Whang, Emily Denton, Seyed Kamyar Seyed Ghasemipour, Burcu Karagol Ayan, S. Sara Mahdavi, Raphael Gontijo-Lopes, Tim Salimans, Jonathan Ho, David J Fleet, and Mohammad Norouzi. Photorealistic text-to-image diffusion models with deep language understanding. In *Advances in Neural Information Processing Systems*, 2022. 1, 3
- [54] Yujun Shen, Jinjin Gu, Xiaoou Tang, and Bolei Zhou. Interpreting the latent space of gans for semantic face editing. In *IEEE/CVF Conference on Computer Vision and Pattern Recognition*, 2020. 3
- [55] Yujun Shen, Ceyuan Yang, Xiaoou Tang, and Bolei Zhou. InterFaceGAN: Interpreting the disentangled face representation learned by gans. *IEEE Transactions on Pattern Analysis and Machine Intelligence*, 2020. 3

- [56] Yujun Shen and Bolei Zhou. Closed-Form factorization of latent semantics in gans. In *IEEE/CVF Conference on Computer Vision and Pattern Recognition*, pages 1532–1540, June 2021. [3](#)
- [57] Yichen Sheng, Zixun Yu, Lu Ling, Zhiwen Cao, Xuaner Zhang, Xin Lu, Ke Xian, Haiting Lin, and Bedrich Benes. Dr. Bokeh: Differentiable occlusion-aware bokeh rendering. In *IEEE/CVF Conference on Computer Vision and Pattern Recognition*, pages 4515–4525, June 2024. [5](#)
- [58] Yichun Shi, Peng Wang, Jiangleong Ye, Long Mai, Kejie Li, and Xiao Yang. MVDream: Multi-view diffusion for 3d generation. *arXiv preprint arXiv:2308.16512*, 2023. [4](#)
- [59] Yang Song, Jascha Sohl-Dickstein, Diederik P Kingma, Abhishek Kumar, Stefano Ermon, and Ben Poole. Score-based generative modeling through stochastic differential equations. In *International Conference on Learning Representations*, 2021. [1](#), [2](#)
- [60] Wenqiang Sun, Shuo Chen, Fangfu Liu, Zilong Chen, Yueqi Duan, Jun Zhang, and Yikai Wang. DimensionX: Create any 3d and 4d scenes from a single image with controllable video diffusion, 2024. [3](#)
- [61] Omer Tov, Yuval Alaluf, Yotam Nitzan, Or Patashnik, and Daniel Cohen-Or. Designing an encoder for StyleGAN image manipulation. *ACM Transactions on Graphics*, 40(4), 2021. [3](#)
- [62] Zhouxia Wang, Ziyang Yuan, Xintao Wang, Yaowei Li, Tianshui Chen, Menghan Xia, Ping Luo, and Ying Shan. Motionctrl: A unified and flexible motion controller for video generation. In *ACM SIGGRAPH 2024 Conference Papers*, pages 1–11, 2024. [3](#)
- [63] Andrew P. Witkin. Scale-space filtering. In *Readings in Computer Vision*, pages 329–332. 1987. [5](#), [12](#)
- [64] Krzysztof Wolski, Adarsh Djeacoumar, Alireza Javanmardi, Hans-Peter Seidel, Christian Theobalt, Guillaume Cordonnier, Karol Myszkowski, George Drettakis, Xingang Pan, and Thomas Leimkühler. Learning images across scales using adversarial training. *ACM Transactions on Graphics*, 43(4), 2024. [5](#)
- [65] Chen Wu and Fernando De la Torre. Contrastive prompts improve disentanglement in text-to-image diffusion models. *arXiv preprint arXiv:2402.13490*, 2024. [3](#)
- [66] Qiucheng Wu, Yujian Liu, Handong Zhao, Ajinkya Kale, Trung Bui, Tong Yu, Zhe Lin, Yang Zhang, and Shiyu Chang. Uncovering the disentanglement capability in text-to-image diffusion models. In *IEEE/CVF Conference on Computer Vision and Pattern Recognition*, pages 1900–1910, 2023. [3](#)
- [67] Yiming Xie, Chun-Han Yao, Vikram Voleti, Huaizu Jiang, and Varun Jampani. SV4D: Dynamic 3d content generation with multi-frame and multi-view consistency. *arXiv preprint arXiv:2407.17470*, 2024. [4](#)
- [68] Dejie Xu, Yifan Jiang, Chen Huang, Liangchen Song, Thorsten Gernoth, Liangliang Cao, Zhangyang Wang, and Hao Tang. Cavia: Camera-controllable multi-view video diffusion with view-integrated attention. *arXiv preprint arXiv:2410.10774*, 2024. [3](#)
- [69] Dejie Xu, Weili Nie, Chao Liu, Sifei Liu, Jan Kautz, Zhangyang Wang, and Arash Vahdat. CamCo: Camera-controllable 3d-consistent image-to-video generation. *arXiv preprint arXiv:2406.02509*, 2024. [3](#)
- [70] Lihe Yang, Bingyi Kang, Zilong Huang, Xiaogang Xu, Jiashi Feng, and Hengshuang Zhao. Depth Anything: Unleashing the power of large-scale unlabeled data. In *IEEE/CVF Conference on Computer Vision and Pattern Recognition*, 2024. [5](#), [12](#)
- [71] Lihe Yang, Bingyi Kang, Zilong Huang, Zhen Zhao, Xiaogang Xu, Jiashi Feng, and Hengshuang Zhao. Depth Anything v2. *arXiv preprint arXiv: 2406.09414*, 2024. [5](#), [12](#)
- [72] Shiyuan Yang, Liang Hou, Haibin Huang, Chongyang Ma, Pengfei Wan, Zhang Di, Xiaodong Chen, and Jing Liao. Direct-a-Video: Customized video generation with user-directed camera movement and object motion. In *ACM SIGGRAPH 2024 Conference Papers*, page 12, 2024. [1](#)
- [73] Lvmin Zhang, Anyi Rao, and Maneesh Agrawala. Adding conditional control to text-to-image diffusion models, 2023. [1](#), [3](#), [6](#)
- [74] Richard Zhang, Phillip Isola, Alexei A Efros, Eli Shechtman, and Oliver Wang. The unreasonable effectiveness of deep features as a perceptual metric. In *IEEE/CVF Conference on Computer Vision and Pattern Recognition*, 2018. [6](#), [14](#)
- [75] Xuaner Zhang, Qifeng Chen, Ren Ng, and Vladlen Koltun. Zoom to learn, learn to zoom. In *IEEE/CVF Conference on Computer Vision and Pattern Recognition*, 2019. [6](#), [12](#), [13](#)
- [76] Xuaner Zhang, Kevin Matzen, Vivien Nguyen, Dillon Yao, You Zhang, and Ren Ng. Synthetic defocus and look-ahead autofocus for casual videography. *ACM Transactions on Graphics*, 2019. [6](#)

Supplementary Materials

6. Introduction

This supplementary material provides additional discussions and details on the construction of contrastive data (Section 7), network design (Section 8), evaluation metrics (Section 9), and more visual results (Section 10).

To better illustrate the continuity and effects of camera intrinsic setting control, we highly recommend readers view the **Videos/GIFs** provided in the project page at <https://generative-photography.github.io/project/>.

7. More Details of Building Contrastive Data

Our contrastive data pipeline dynamically generates training data by storing only base images and scene descriptions. Camera settings are sampled during training and simulated **on-the-fly** using physical principles, producing contrastive multi-frame data without pre-storing large video files. This also ensures continuous sampling of training data.

We provide below additional key considerations for constructing contrastive datasets for each type of camera setting, along with sample demonstrations.

7.1. Contrastive Data for Bokeh Rendering

As shown in Fig. 6, to enhance the prominence of the bokeh rendering effect, we impose the following two requirements on the base images: 1). The images should be nearly all-in-focus. 2). They should exhibit significant depth differences, allowing clear distinction between foreground and background.

We employ bokehMe [45] for realistic bokeh simulation. During this process, the value of the refocused disparity is consistently maintained at the depth of the foreground.

7.2. Contrastive Data for Focal Length

In the real world, obtaining a set of images of the same scene at multiple focal lengths is highly cumbersome, with a lack of perfect alignment between the images, and the achievable focal length range is limited [75]. In this paper, we reference the level-of-detail [40, 63] approach and compute the field-of-view (FoV) ratio of the desired focal length relative to the base image focal length. This ratio is then used for center cropping to approximate the actual continuous optical zoom process. In this subsection, we compare the performance of our method with that of actual optical zoom. A camera’s field-of-view (FoV) can be expressed in terms of the focal length f and the sensor dimensions (typ-

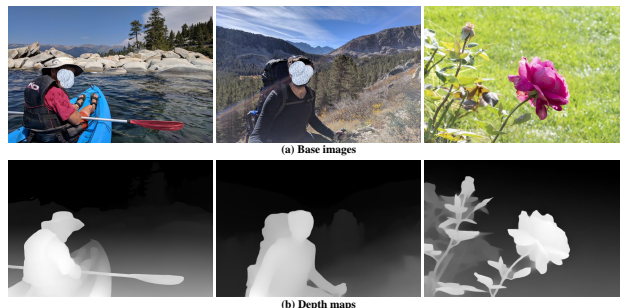


Figure 6. The first row shows examples of base images used for constructing bokeh rendering data, featuring prominent foregrounds and distinguishable backgrounds. The second row presents depth maps extracted using the Depth Anything [70, 71] model.

ically width w or height h). The formulas are as follows: Horizontal FoV:

$$\text{FoV}_h = 2 \cdot \arctan\left(\frac{w}{2f}\right) \quad (1)$$

Vertical FoV:

$$\text{FoV}_v = 2 \cdot \arctan\left(\frac{h}{2f}\right) \quad (2)$$

Diagonal FoV:

$$\text{FoV}_d = 2 \cdot \arctan\left(\frac{\sqrt{w^2 + h^2}}{2f}\right) \quad (3)$$

where w denotes the width of the sensor, h is the height of the sensor, and f represents the focal length.

Based on the aforementioned FoV calculation formula, we crop the central region of a high-resolution base image to simulate the corresponding view at larger focal lengths. Fig. 7 compares the optical zoom with the results generated by our cropping method. The real-world data for different focal lengths is from [75]. Our method demonstrates a high degree of consistency with the real data in terms of FoV. It is worth noting that due to the resolution and quality constraints of the base image, excessive cropping leads to significant loss of detail and quality. Therefore, in this work, we limit the focal length range to 24-70mm.

7.3. Contrastive Data for Shutter Speed

A realistic imaging model can be formulated as follows, similar to [12, 36, 47]. Consider a final LDR image, L , cap-

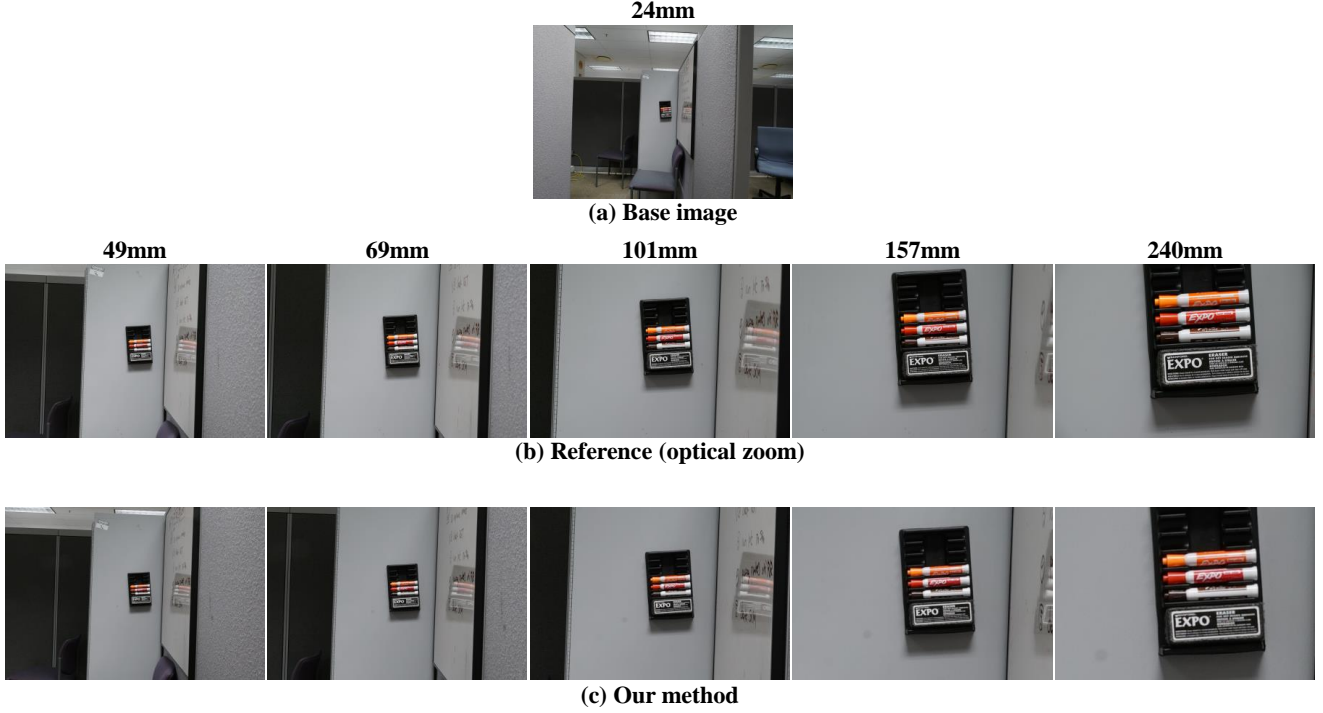


Figure 7. The comparison between the reference real focal lengths and our simulated results. Note that the real-world shooting data is derived from [75], and there may be slight misalignment between images of different resolutions due to shooting conditions. We observe that excessively high focal length simulation ratios can lead to a decline in image quality. Therefore, in this study, the focal length range is constrained to 24-70mm. Please zoom in for a more detailed comparison.

tured at an exposure time of t where the underlying HDR scene irradiance map is represented by H .

$$L = \text{ADC} \left\{ \xi \times \text{Clip} \left\{ \text{Poisson} \left(t \times \text{QE} \times (H + \mu_{\text{dark}}) \right) \right. \right. \\ \left. \left. + N(0, \sigma_{\text{read}}^2) \right\}^{1/\gamma} \right\} \quad (4)$$

where ξ is the conversion gain, QE is the quantum efficiency, μ_{dark} is the dark current, and σ_{read} is the read noise standard deviation. Here, Poisson represents the Poisson distribution characterizing the photon arriving process and the dark current effect, and N represents the Gaussian distribution characterizing the sensor noise. $\text{ADC} \{ \cdot \}$ is the analog-to-digital conversion and $\text{Clip} \{ \cdot \}$ is the full well capacity induced saturation effect. We assume a linear camera response function for CMOS sensors and that the imperfections in the pixel array, ADC, and color filter array have been mitigated.

For the shutter speed control task, we selected base images with a high dynamic range and appropriate exposure to approximate H . By varying the parameter t in the formula 4, we simulate multiple frames corresponding to different shutter speeds.

7.4. Contrastive Data for Color Temperature

We employ an empirical approximation revised from [14] to map a given color temperature in Kelvin to corresponding RGB values, ensuring accurate and balanced color representation. The input kelvin is normalized by dividing by 100, resulting in temp. The conversion process is as follows:

For $\text{temp} \leq 66$:

$$\text{RGB} = (255, \\ \max(0, 99.47 \cdot \ln(\text{temp}) - 161.12), \\ \max(0, 138.52 \cdot \ln(\text{temp} - 10) - 305.04)) \quad (5)$$

For $66 < \text{temp} \leq 88$:

$$\text{RGB} = (0.5 \cdot (255 + 329.70 \cdot (\text{temp} - 60)^{-0.1933}), \\ 0.5 \cdot (288.12 \cdot (\text{temp} - 60)^{-0.1155} \\ + 99.47 \cdot \ln(\text{temp}) - 161.12), \\ 0.5 \cdot (138.52 \cdot \ln(\text{temp} - 10) - 305.04 + 255)) \quad (6)$$

For $\text{temp} > 88$:

$$\begin{aligned} \mathbf{RGB} = & (329.70 \cdot (\text{temp} - 60)^{-0.1933}, \\ & 288.12 \cdot (\text{temp} - 60)^{-0.1155}, \\ & 255) \end{aligned} \quad (7)$$

After computation, the RGB values are clipped to the range $[0, 255]$ to ensure valid color values. The resulting balanced RGB values are returned as a `float32` array, providing an accurate representation of the input temperature in RGB space.

8. More Details of Contrastive Camera Encoder

In the Contrastive Camera Encoder, an important aspect is the incorporation of the differences in camera setting scales. We extract the camera settings for F_r frames using the CLIP text encoder, compute the differences, and then reshape the result into an embedding of size $F_r \times C \times H \times W$.

In addition, this section will also provide more details on the coarse embedding and the embedding encoder.

8.1. Coarse Embedding

The input to the coarse embedding is solely the provided camera settings. Based on a simplified version of the physical simulation model, it outputs an embedding with a shape of $F_r \times C \times H \times W$.

For bokeh rendering, the input bokeh blur parameter is treated as an equivalent Gaussian blur kernel. A larger parameter indicates that the weight of each pixel in the output is lower, resulting in smaller global pixel embedding values.

As illustrated in Fig. 8, for focal length, we use mask to proxy the coarse embedding. Specifically, after calculating the field of view (FoV) ratio, we mask out regions of the original image resolution that should not be present.



Figure 8. We use a mask as the coarse embedding for focal length control. The black areas represent pixels around the edges of the frame that should not be displayed at the given focal length.

For shutter speed, we roughly estimate the ratio between the target shutter time and the base shutter time (simplified as 0.2 second on average). This ratio is then used to compute the overall average brightness ratio of the image, which serves as the global coefficient for the coarse embedding.

For color temperature, we estimate the ratio coefficients for the RGB channels based on the color temperature value, using a simplified version of the corresponding formula from

Equation 5 to Equation 7. These coefficients are then used as the scaling factors for the coarse embedding.

8.2. Embedding Encoder

The embedding encoder takes both the coarse embedding and the differential information embedding as input. After encoding, it injects the information into the temporal attention layers of the foundation model in a hierarchical manner. Its internal structure is based on the T2I adapter [42], with additional temporal structures for multi-setting processing.

9. More Details of Metrics

9.1. Accuracy

To evaluate the accuracy of the camera physics in generated images, we first simulate the reference frames of the base image under multiple camera settings, using the same scene description and corresponding camera parameters for generation. We then calculate the overall trend of camera effects within the reference frames and the overall trend of camera effects within the generated multi-frame sequence. The Pearson correlation coefficient between these two trends is computed as an accuracy metric (CorrCoef). For each type of camera setting, we employ different methods to calculate the camera effects.

- For Bokeh: We compute the average blur level per frame using the Laplacian operator.
- For Focal Length: We first detect feature points using SIFT [38], then perform feature matching between adjacent frames using Brute-Force Matcher [1]. We calculate the similarity transformation matrix from the matched points and extract the scaling factor from the transformation matrix.
- For Shutter Speed: We compute the average brightness per frame.
- For Color Temperature: We compute the average color per frame.

9.2. Consistency

For the consistency between frames corresponding to different camera setting values, we compute the frame-to-frame consistency using the Frame-wise Learned Perceptual Image Patch Similarity (LPIPS) [74]. Subsequently, we average the LPIPS scores of all adjacent frames to obtain the final score. An important nuance here is that a lower LPIPS score is not always preferable, as we require some variation in camera effects. Therefore, the LPIPS score should be compared to that of reference videos, with a closer match indicating better performance.

9.3. Quality

We measure the quality of the generated frames by evaluating their alignment with the input prompts. Specifically, we use the CLIP [48] text and image encoders to obtain the features of the prompt and the generated frame, and then compute the cosine similarity between the two.

10. More Visual Results

In this section, we provide additional visual results and comparisons with other methods.

Fig. 9 to Fig. 12 illustrate the visual comparisons for bokeh rendering, focal length, shutter speed, and color temperature across various generative methods. Our approach demonstrates significant advantages in understanding camera physical parameters while maintaining scene consistency.

We strongly encourage readers to view the videos (GIFs) on project page for more intuitive comparisons and additional case studies.

Bokeh Rendering

A display of frozen desserts, including cupcakes and donuts, is arranged in a row on a counter. The desserts are placed in plastic containers, and there are several of them in various sizes and flavors; with bokeh blur parameter **

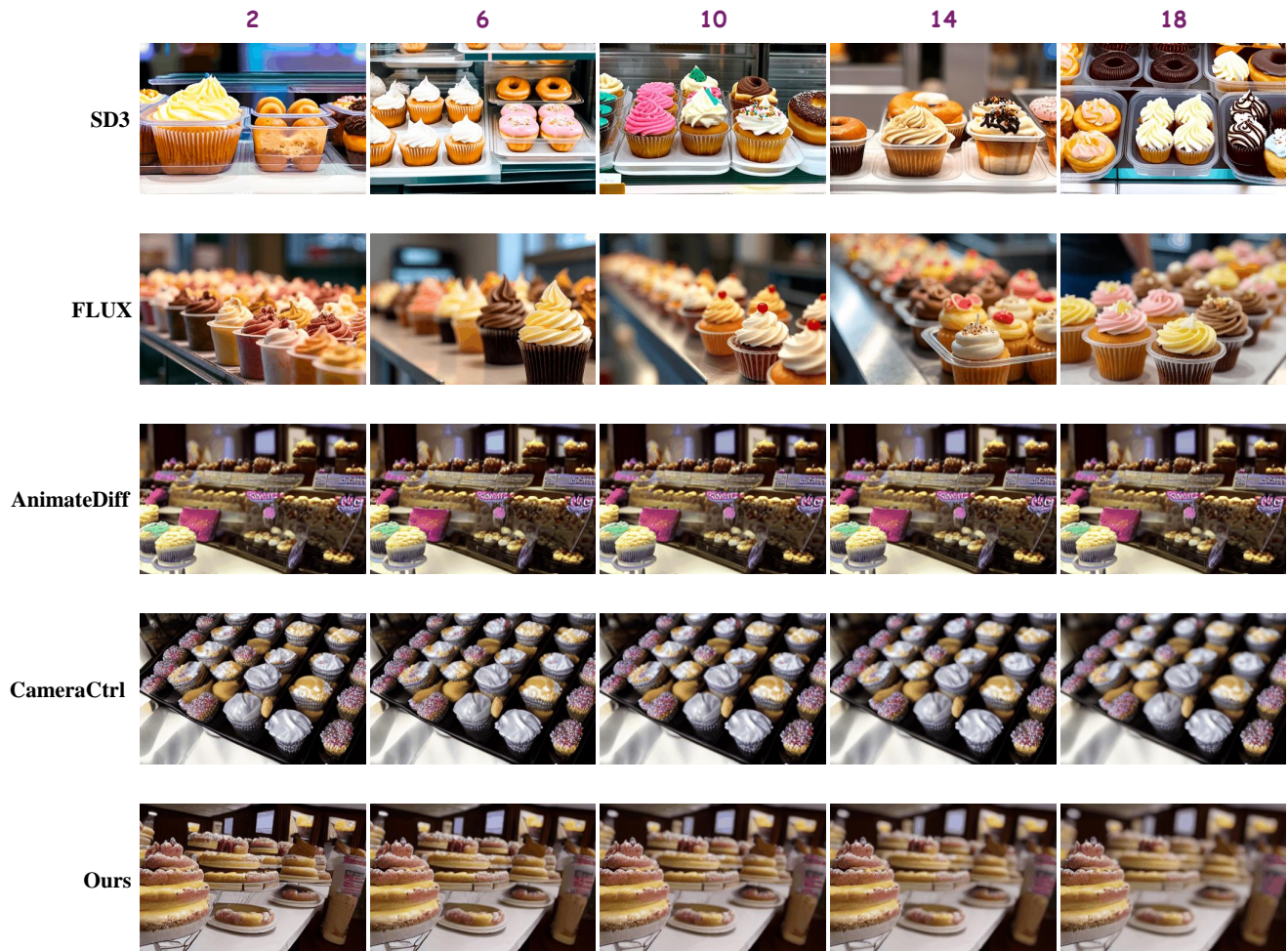


Figure 9. Visual comparisons between different generative methods on camera bokeh rendering control. Both AnimateDiff [20] and CameraCtrl [22] have been fine-tuned/trained on our data.

Focal Length

A clean beach with a few footprints;
with ** lens

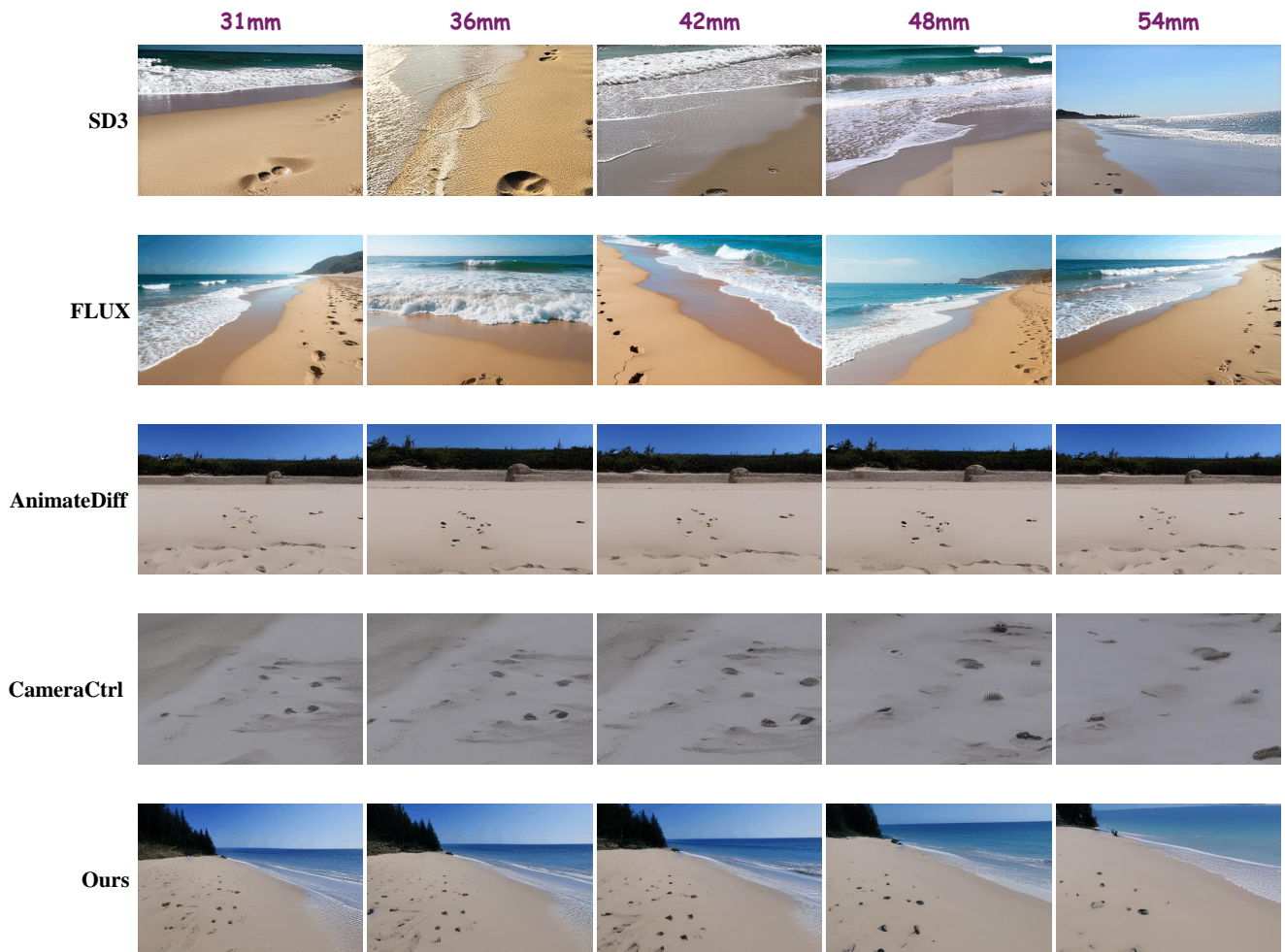


Figure 10. Visual comparisons between different generative methods on camera focal length control. Both AnimateDiff [20] and CameraCtrl [22] have been fine-tuned/trained on our data.

Shutter Speed

A kitchen with a black countertop and a window above the sink. The kitchen is well-equipped with a microwave, oven, and various utensils such as knives and spoons; with shutter speed **

0.2 second

0.36 second

0.46 second

0.66 second

0.85 second

SD3



FLUX



AnimateDiff



CameraCtrl



Ours



Figure 11. Visual comparisons between different generative methods on camera shutter speed control. Both AnimateDiff [20] and CameraCtrl [22] have been fine-tuned/trained on our data.

Color Temperature

A beautiful view of a city with a castle and a large body of water;
with temperature **

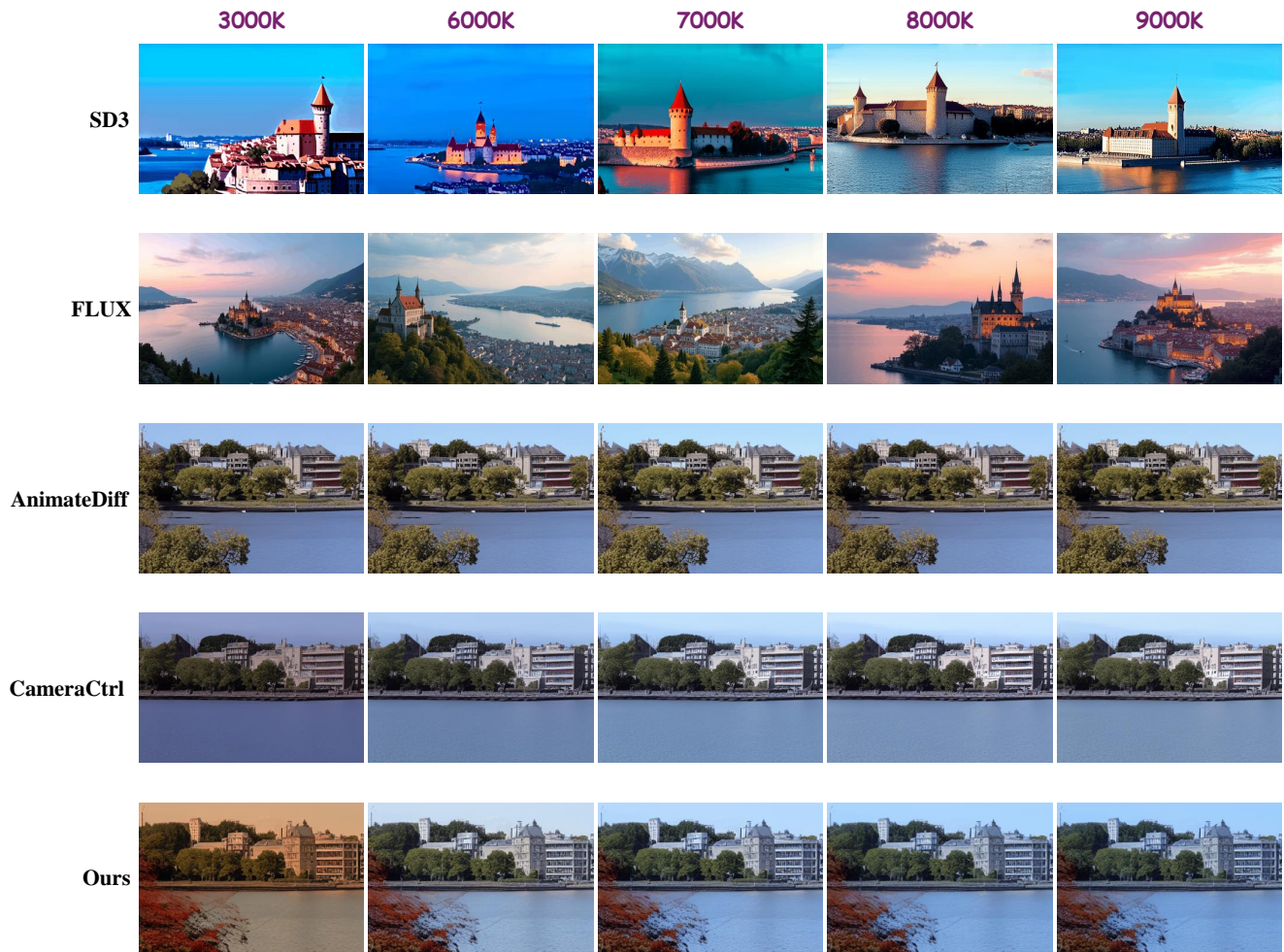


Figure 12. Visual comparisons between different generative methods on camera focal length control. Both AnimateDiff [20] and CameraCtrl [22] have been fine-tuned/trained on our data.